

Nonlinear denoising for characterization of solid friction under low confinement pressure

Jules Colas, Nelly Pustelnik, Cristobal Oliver, Patrice Abry, Jean-Christophe Géminard, Valérie Vidal

▶ **To cite this version:**

Jules Colas, Nelly Pustelnik, Cristobal Oliver, Patrice Abry, Jean-Christophe Géminard, et al.. Nonlinear denoising for characterization of solid friction under low confinement pressure. Physical Review E , 2019, 42, pp.91. 10.1103/PhysRevE.100.032803 . hal-02271333

HAL Id: hal-02271333
https://hal.science/hal-02271333

Submitted on 26 Aug 2019

HAL is a multi-disciplinary open access archive for the deposit and dissemination of scientific research documents, whether they are published or not. The documents may come from teaching and research institutions in France or abroad, or from public or private research centers.

L'archive ouverte pluridisciplinaire **HAL**, est destinée au dépôt et à la diffusion de documents scientifiques de niveau recherche, publiés ou non, émanant des établissements d'enseignement et de recherche français ou étrangers, des laboratoires publics ou privés.

Nonlinear denoising for characterization of solid friction under low confinement pressure

Jules Colas[1], Nelly Pustelnik[1], Cristobal Oliver[2], Patrice Abry[1], Jean-Christophe Géminard[1], Valérie Vidal[1]
[1] *Univ Lyon, ENS de Lyon, Univ Lyon 1, CNRS, Laboratoire de Physique, Lyon, France*
[2] *Instituto de Fisica, Pontificia Universidad Católica de Valparaiso, Av. Universidad 330, Valparaiso, Chile*
(Dated: July 29, 2019)

The present work investigates paper-paper friction dynamics by pulling a slider over a substrate. It focuses on the transition between stick-slip and inertial regimes. Although the device is classical, probing solid friction with the fewest contact damage requires that the applied load should be small. This induces noise, mostly impulsive in nature, on the recorded slider motion and force signals. To address the challenging issue of describing the physics of such systems, we promote here the use of nonlinear filtering techniques relying on recent nonsmooth optimization schemes. In contrast to linear filtering, nonlinear filtering captures the slider velocity asymmetry and, thus, the creep motion before sliding. Precise estimates of the stick and slip phase durations can thus be obtained. The transition between the stick-slip and inertial regimes is continuous. Here we propose a criterion based on the probability of the system to be in the stick-slip regime to quantify this transition. A phase diagram is obtained that characterizes the dynamics of this frictional system under low confinement pressure.

I. INTRODUCTION

Since the first reports by Leonardo da Vinci in 1493 [1], frictional properties of solids are inferred from classical experiments, where a slider of mass m, imposing a normal load to the substrate, is pulled over a fixed substrate. Starting from a slider at rest, the pulling force has to increase above a threshold value to trigger the slider motion. The slider then slips over a given distance, then stops. This dynamics, referred to as "stick-slip", has later been investigated by Amontons (17th century) and Coulomb (18th century) [2]. In the last decades, systematic studies have considered a slider pulled at average constant driving velocity V by means of a spring of stiffness k. Monitoring the force F applied to the slider in time thus provides a direct access to the slider dynamics, and to the frictional properties of the material. In the simplified framework of Amontons-Coulomb [3, 4], starting from a slider initially at rest (*stick* phase), the force F increases linearly with a slope proportional to kV (Fig. 1a). Once a given threshold is reached (Fig. 1a, white dot), the load starts sliding (*slip* phase). The duration of the stick, τ_{st}, and slip, τ_{sl}, phases are controlled by the experimental parameters (m, k, V). In particular, the characteristic time of motion, $\tau_m = \tau_{sl}$ in this simplistic model, almost equals $T = \pi\sqrt{m/k}$, i.e. half the period of the spring-mass system (or inertial time).

However, the comparison of this simple model with experiments reveals several limitations. First, the determination of the time during which the slider is in motion is rather difficult. Indeed, the start of the slip motion does not correspond to the maximum of the force signal (Fig. 1a, white dot), and its stop does not correspond to the minimum (Fig. 1a, gray dot). Moreover, the creep introduces an additional contribution, τ_c, to the total time during which the slider is indeed in motion, $\tau_m = \tau_c + \tau_{sl}$ (Fig. 1b). Therefore, the accurate determination of the start and stop times is challenging, especially when the experimental data are noisy. Second, the frictional properties have been shown to depend on the contact time between the surfaces, and on the sliding velocity [3–8]. Although this so-called rate-and-state modeling is now widely recognized, it fails to account for the variations in the friction coefficients due to spatial heterogeneities of the material [9, 10], which may lead, for a given material, to distributed values of (τ_{st},τ_{sl}) rather than to single values. Third, it is of particular interest to consider the limit of vanishing normal load, in particular to avoid polishing which damages surfaces and alters of the local frictional properties. We thus are interested in the frictional properties of materials easily worn by shear

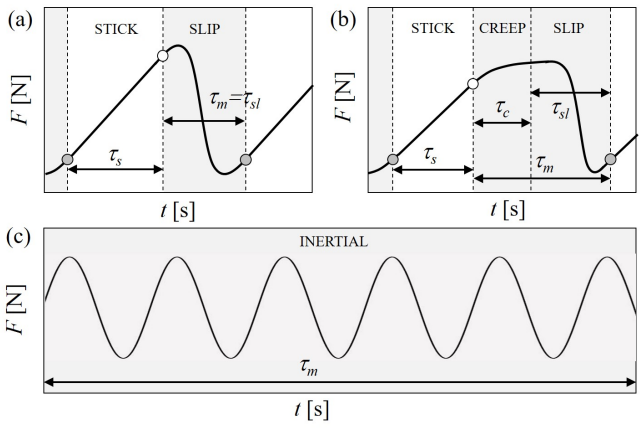


FIG. 1. Different solid friction dynamics. (a) Stick-slip motion without creep. (b) Stick-slip motion with significant creep. (c) Inertial motion [In panels (a), (b) and (c), F denotes the force applied to the slider pulled at average constant driving velocity V by means of a spring of stiffness k. We denote τ_{st} and τ_{sl} the stick and slip phase durations, τ_c the creep duration and τ_m the total time during which the slider is in motion (gray region)].

at loads far smaller than considered in previous studies [11], which is still an open practical challenge. Indeed, the use of very small normal loads induces a significant noise, often impulsive in nature, in the recorded signals. Furthermore, experimental data with low signal-to-noise ratio often imply using sensitive recording devices, which may be subjected to additional electronic noise.

The aforementioned problems yield significant issues in the analysis of the empirical data recorded to characterize the slider dynamics. For small k and V, the slider exhibits the typical stick-slip motion previously described (Figs. 1a and 1b). However, when V is increased, the system undergoes a transition to an inertial regime, where the temporal force variations remain periodic, but no longer show stick phases (Fig. 1c) [11, 12]. Other transitions to continuous sliding are also reported for large V in the case of granular friction [13] or for small V and large k in the case of dry solid friction, the dynamics being dominated by the creep in this limit [11, 14]. Although a transition from stick-slip to continuous sliding is easy to identify, thanks to the disappearance of the periodicity, the transition between stick-slip and inertial regimes remains far more difficult to detect, especially with noisy experimental signals, wide distributions of (τ_{st},τ_{sl}) and the possible presence of creep.

The contribution of this work is twofold. First, to extract information from the experimental data, we promote the use of nonlinear filtering techniques, relying on recent nonsmooth optimization schemes, and show their benefits compared to classical linear filtering. Linear and nonlinear filtering techniques are thus compared to denoise the temporal variations of the force signal, collected on paper-paper friction experiments under small normal loads (Sec. II). Contrary to the classical linear filtering, nonlinear filtering is shown to successfully capture creep motion before sliding and to filter a large part of the impulsive noise, thus permitting a better detection of the stick and slip phases (Sec. III). Second, the proposed nonlinear analysis scheme is systematically applied to 189 experiments, obtained by varying k and V (Sec. IV). This nonlinear filtering permits to precisely investigate the transition between the stick-slip and inertial regimes, and how the system undergoes this transition when varying the experimental parameters. A phase diagram is finally devised in the $k - V$ plane describing the frictional properties of the paper-paper system under study.

II. EXPERIMENT & DATA ACQUISITION

A. Experimental setup

The experimental setup consists of a slider pulled over a solid substrate via a cantilever spring (Fig. 2). The surface area of the slider, 9×6 cm^2, and its mass, $m = 30.7$ g, are chosen to avoid excessive wear of the sliding surfaces by working at small normal stress (about 56 Pa). We point out that previous studies, although working with a similar setup, used a larger slider mass (300 g) and an additional load of the order of 1000 g, corresponding to far larger normal stresses of about 1300 Pa [11]. The contact between the cantilever spring (metallic blade, stiffness k) and the slider is ensured by a steel sphere glued to the slider. This allows the free motion of the contact point. The blade is translated at constant velocity V, and its deflection Δx is measured by an inductive sensor (Baumer, IPRM 12I9505/S14). The spring stiffness is varied between $k = 168$ and 3337 N/m and the driving velocity V between 42 and 7200 μm/s.

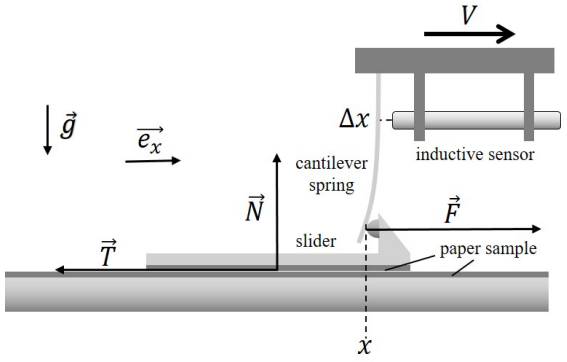


FIG. 2. Experimental setup. A cantilever spring of stiffness k is pulled at constant velocity V at one end, and entrains a slider of mass m at the other end. The deflection Δx of the cantilever spring, measured by an inductive sensor, provides simultaneously the velocity of the slider in the frame of the laboratory, $\dot{x} = V - \Delta\dot{x}$, and the force, $F \equiv k\,\Delta x$, applied to it. We denote $\vec{T}$ the tangential (friction) force and $\vec{N}$ the normal load.

The substrate and the bottom surface of the slider are coated with Canson® sheets, a drawing paper characterized by a rough surface. Even for the chosen small normal load, the surfaces exhibit undesired wear after repeated experiments. Note that in Heslot *et al.* [11] the absence of wear at larger normal load was attributed to the properties of the Bristol board in use. To ensure reproducibility, we perform 3 experimental runs for a given set of parameters (k, V). We then change the samples, check for the same (k, V) that the force signal has the same characteristics, change the parameters (k, V), perform again 3 series of experiments, and so on.

B. Data acquisition

From the blade deflection Δx, after an appropriate calibration procedure, the force F applied to the slider is reconstructed as $F \equiv k\,\Delta x$ (Fig. 2). For each set of parameters (k, V), the force signal is recorded over a total slider displacement of about 1.5 cm, with a sampling frequency of 2 kHz. The signal size thus varies from about 7.5×10^5 to 4.5×10^3 sample points. In the following, we use the normalized force signal, F/mg, where $g = 9.81$ m.s^{-2} is

the gravitational acceleration.

To quantify the system dynamics - and, therefore, the frictional regime - we consider the slider velocity, $\dot{x} = V - \Delta\dot{x}$, which can be rewritten as:

$$\dot{x} = V - \frac{1}{k}\frac{\mathrm{d}F}{\mathrm{d}t}\,. \tag{1}$$

Computing empirically a relevant derivative, and hence an accurate estimate of the velocity, obviously requires an efficient denoising of the force signal. The velocity $\dot{x}$ will be further used to detect slip events and estimate accurately, for each event, the stick, creep and slip time τ_{st}, τ_c and τ_{sl}. Here, the slip (or sliding) phase does not include creep. The total time during which the slider is in motion is therefore $\tau_m = \tau_c + \tau_{sl}$, as displayed in Fig. 1b.

Considering the 9 driving velocities, 7 spring stiffnesses and 3 runs for each set of parameters, the total amount of experiments and, therefore, signals to analyze, is 189.

III. NONLINEAR DENOISING

The challenge in working at small normal loads is the poor signal to noise ratio, which requires a careful signal analysis to quantify the physical properties of the system. Solid friction dynamics is classically studied by means of low-pass linear filtering for denoising the force signal prior to computing the velocity. The drawback of such linear filtering is not only to remove the noise but also to alter a relevant high-frequency part of the friction dynamics, especially during the stick-slip regime. To overcome this limitations stemming from linear filtering, we propose here to use nonlinear filtering techniques, relying on nonsmooth optimization schemes. We devise corresponding iterative minimization algorithms that benefit both from reasonable computational costs, thus permitting the analysis of large-size signals, and from theoretical recovery and convergence guarantees [15, 16].

A. Force denoising and event detection

1. Principle

Linear filtering – Let f_{obs} denote the normalized force signal to analyze, $f_{\mathrm{obs}} = F/mg$, of size N samples. Linear filtering consists of a convolution with a filter h [17],

$$\widehat{f}_{Lin} = h * f_{\mathrm{obs}}. \tag{2}$$

Linear filtering can also be rewritten as a minimization problem,

$$\widehat{f}_{Lin} = \arg\min_f \frac{1}{2}\|f - f_{\mathrm{obs}}\|_2^2 + \lambda\|Hf\|_2^2 \tag{3}$$

$$= (\mathrm{Id} + 2\lambda H^\top H)^{-1} f_{\mathrm{obs}} \tag{4}$$

where $\|\cdot\|_2^2$ is the usual euclidean norm and $(\mathrm{Id} + 2\lambda H^* H)^{-1}$ is the matrix of size $N \times N$ associated with the shape of filter h. Parameter $\lambda > 0$ essentially controls the width of the band of the low-pass filter h.

Nonlinear filtering – To remove high frequency noise while keeping sharp discontinuities in signals, it has been proposed in the inverse problem literature to replace the ℓ_2-norm with a ℓ_1-norm ($\|u\|_1 = \sum_i |u_i|$) in the filtering term [18]:

$$\widehat{f}_{NonLin} = \arg\min_f \frac{1}{2}\|f - f_{\mathrm{obs}}\|_2^2 + \lambda\|Hf\|_1. \tag{5}$$

When using a finite difference (increment) filter $h = [-1, +1]$, such nonlinear filtering yields piecewise constant estimates $\widehat{f}_{NonLin}$ [18]. However, in the context of friction data, the force signal is better approximated with piecewise linear estimates (notably in the stick-slip regime). Therefore, we propose to use Laplacian filters ($h = [-1, 2, -1]$) that favor such behaviors.

2. Iterative algorithms

The main issue in practically implementing nonlinear filtering as in Eq. (5) above lies in the absence of closed form solution for $\widehat{f}_{NonLin}$, thus implying the recourse to iterative algorithms to minimize the corresponding functional, leading to potentially high computational costs. In addition, the non differentiability of the functional to minimize induced by the use of the ℓ_1-norm precludes the use of gradient descent algorithms. Instead, gradient operators need to be replaced with proximity operators [16, 20]. Finally, the large data size ($N \sim 10^6$) of friction signals requires the use of fast algorithms. Therefore, we have devised Algorithm 1, that relies on the use of the notion of strong convexity into primal-dual proximal scheme to achieve fast minimization of Eq. (5), via a sequence $(f^{[k]})_{k\in\mathbb{N}}$ that converges to $\widehat{f}_{NonLin}$ with linear convergence rate [19, 20]. The proximity operator of the ℓ_1-norm consists of a soft-thresholding operation [16, 21], with $\gamma > 0$,

$$\mathrm{prox}_{\gamma\|\cdot\|_1}(u) = \begin{cases} u_i - \gamma & \text{if} \quad u_i > \gamma, \\ u_i + \gamma & \text{if} \quad u_i < -\gamma, \\ 0 & \text{otherwise.} \end{cases} \tag{6}$$

3. Selection of the regularization parameter λ

In linear filtering, parameter λ essentially acts as the (inverse of the) width of the low-pass filter (Fig. 3). In nonlinear filtering, parameter λ also impacts the solution $\widehat{f}_{NonLin}$: A small λ leads to $\widehat{f}_{NonLin}$ close to the input

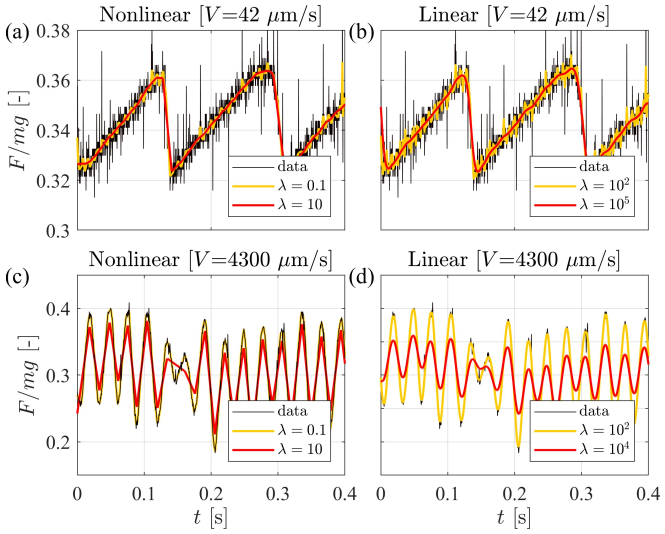


FIG. 3. Examples of nonlinear (a,c) and linear (b,d) filtering for small and large values of the parameter λ. (a,b) Stick-slip regime [$V = 42$ μm/s, $k = 1002$ N/m]. (c,d) Inertial regime [$V = 4300$ μm/s, $k = 1002$ N/m].

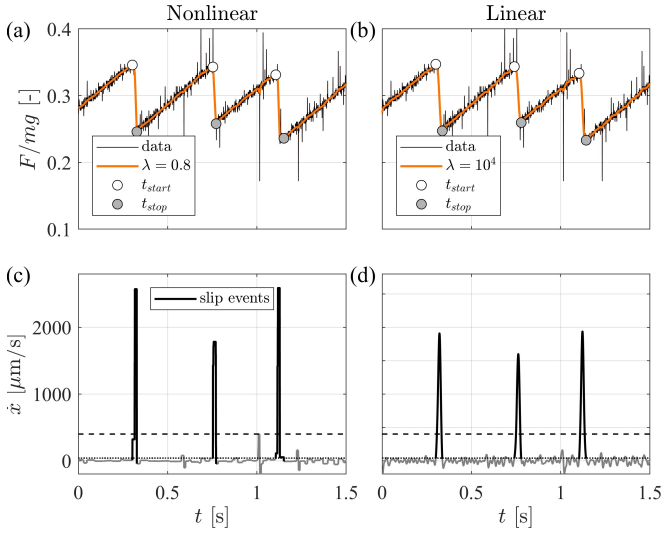


FIG. 4. Normalized force F/mg (a,b) and slider velocity $\dot{x}$ (c,d) obtained from nonlinear (a,c) and linear (b,d) filtering in the stick-slip regime [$V = 70$ μm/s]. The dots in (a) and (b) indicate the start (white dots) and stop (gray dots) of the slider motion [black segments in (c) and (d)]. (c,d) The dashed line indicates the velocity threshold for event detection, and the dotted line the noise level (see text) [$k = 1002$ N/m].

data $f_{\rm obs}$ while a large λ yields piecewise linear estimates, with only a few segments (Fig. 3).

As for linear filtering, automatically tuning the regularization parameter λ in nonlinear filtering to achieve optimal denoising is a complex task. Systematically inspecting the denoised signals obtained from data collected over all 63 different experimental sets of parameters for several λ, permitted to select the optimal λ as the one that better removes noise while preserving the sharp and meaningful changes of the force signals, a slow climb (*stick*) and a fast descent (*slip*). For nonlinear filtering, $\lambda = 0.8$ was found to be robust for all sets of data, while for linear filtering, λ needs to be adjusted to each set of experimental parameters over a wide range, typically between 10^2 to 10^4. For automated selection of λ, we could consider either an empirical rule that consists in setting $\lambda \sim N^{1/2}\sigma/4$ where N is the signal size and σ the noise standard deviation estimated from the median value of the absolute value of the wavelet coefficients [22], or the Stein Unbiased Risk Estimator (SURE) which provides an unbiaised estimator of the mean square error [23–25]. However both techniques fail to provide us with a reliable estimate of λ, the results being too noisy. Note that the empirical rule gives a good order of magnitude of λ for the nonlinear filtering, and could serve as a first estimation of this parameter before its final tuning.

Initialization: Choose $\tau_0, \sigma_0 > 0$ with $\tau_0\sigma_0 \leq 1$

Initialization: Choose $f^{[0]} \in \mathbb{R}^N$, $g^{[0]} \in \mathbb{R}^N$, and $\overline{f}^{[0]} = f^{[0]}$

For $k = 0, 1, \ldots$

$$t^{[k]} = g^{[k]} + \sigma_k H \overline{f}^{[k]}$$

$$g^{[k+1]} = t^{[k]} - \sigma_k \mathrm{prox}_{\frac{\lambda}{\sigma_k}\|\cdot\|_1}\left(\frac{t^{[k]}}{\sigma_k}\right)$$

$$f^{[k+1]} = \frac{1}{1+\tau_k}(f^{[k]} - \tau_k H^\top g^{[k+1]} + \tau_k f_{\rm obs})$$

$$\theta_k = 1/\sqrt{1+2\tau_k},\ \tau_{k+1} = \theta_k\tau_k,\ \sigma_{k+1} = \sigma_k/\theta_k$$

$$\overline{f}^{[k+1]} = f^{[k+1]} + \theta_k(f^{[k+1]} - f^{[k]})$$

Algorithm 1: Proximal primal-dual algorithm.

4. *Event detection*

Figure 4 displays the normalized force F/mg and slider velocity $\dot{x}$ obtained from nonlinear and linear denoising techniques. The automated detection of events, corresponding to a slider motion, is conducted as follows. First, the standard deviation of the base line of the slider velocity is computed and used as a proxy for the noise level on the velocity signal (dotted line, Figs. 4c and 4d). This analysis can be performed only for experiments where the slider exhibits a stick-slip motion. In such experiments, the noise level in the slider velocity is of about 40 μm/s. Second, slip events are detected by thresholding the velocity signal above ten times the noise level (dashed line, Figure 4c,d). Third, motion events (including slip and possible creep motion) are reconstructed by complementing detection on the velocity signal down to the noise level (Figs. 4c and 4d, dark segments). Note that we systematically complemented the velocity signal

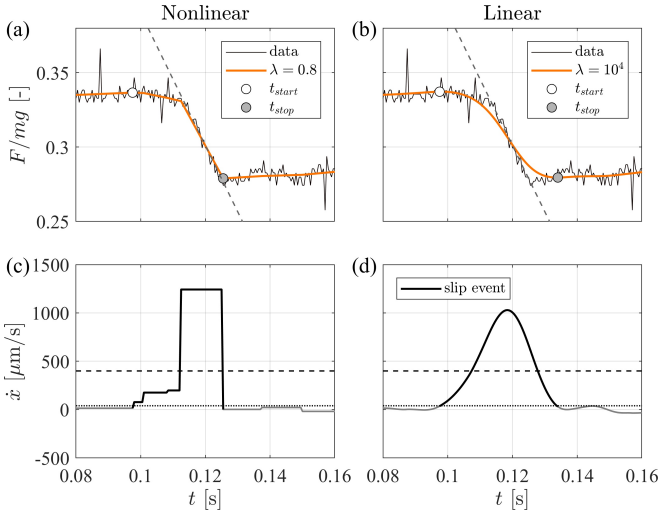


FIG. 5. Example of creep motion before slip. Normalized force signal (a,b) associated with slider velocity (c,d) for nonlinear (a,c) and linear (b,d) filtering. Dashed line in (a,b) is the slope associated with slip on raw experimental data. Dashed and dotted lines in (c,d) indicate the velocity threshold for event detection and the noise level [$k = 1002$ N/m, $V = 42$ μm/s].

down to the first point *below* the noise level, not to miss any abrupt velocity rise or drop which may occur in the vicinity. Due to the signal discretization, the events start and stop may thus appear either very close, or clearly below to the noise level, depending on the local velocity variations (see dark segments in Figs. 4c, for instance). This procedure ensures a relevant detection of the slider motion, its start times t_{start} (white dots, Fig. 4a) and stop times t_{stop} (gray dots, Fig. 4a), thus yielding an accurate quantification, for each event i, of its duration, $\tau_m(i) = t_{stop}(i) - t_{start}(i)$, and of the preceding stick phase, $\tau_{st}(i) = t_{start}(i) - t_{stop}(i-1)$.

B. Nonlinear vs. linear denoising

This section compares the efficiency of the nonlinear versus the linear filtering techniques in analyzing the force signals, with focus i) on the relevance of denoising, ii) on the accuracy in measuring short timescales in slip phases, iii) on detecting creep motion, iv) on detecting whether the slider experiences motion or not (hereafter called "event") and whether the motion is sustained over more than one period of the force signal. This latter quantification will be further necessary to define an accurate criterion for the transition between stick-slip and inertial motion.

1. Denoising

Figs. 3 and 5 clearly illustrate that, while linear filtering can be tuned to filter correctly the experimental impulsive noise, it also significantly smooths out sharp changes in the force signals, hence precluding a relevant analysis of the temporal dynamics in frictional motion, notably a correct estimation of the slip duration. To the contrary, nonlinear filtering as defined in Eq. (5), both removes noise and preserves the features of the force signal that are meaningful for friction temporal dynamics.

2. Creep and slip phases

Fig. 5 further focuses on a single event, for an experiment at small driving velocity ($V = 42$ μm/s). As often encountered experimentally (see Fig. 1b), the slider exhibits a slow motion (creep) before the slip phase. Classical techniques of event detection by picking the maximum and minimun of the force signal find here their limit. Indeed, the creep motion can have a duration comparable to or even larger than that of the slip phase (Figs. 5a and 5c). Not detecting this slow motion would lead to an incorrect estimate of the stick duration, as well as of the duration of the slider motion (creep + slip). Although the nonlinear filtering provides by definition a stepped velocity signal (Fig. 5c), it captures successfully both the slope of the force drop and the creep motion previous to the slip, visible via a strong asymmetry in $\dot{x}$ when the slider moves. Conversely, the linear filtering provides a smoother signal, but smooths the force drop too much (Fig. 5b). Hence, it does not capture neither the correct slope nor the velocity asymmetry (Fig. 5d). Not only no creep motion can be detected here, but the duration of the slider motion is overestimated because of the decrease in the slope of the force drop associated with the slip event (gray dashed line, Fig. 5c).

Figs. 6a and 6b show further examples of nonlinear (a) and linear (b) filtering applied to the force signals in the stick-slip regime. As in previous figures, the white and gray dots indicate the detection of the start and stop of motion events (including possible creep). The creep and slip phases can be measured as:

$$\tau_c = (t_{stop} - t_{start}) - T \quad (7)$$

$$\tau_{sl} = 2(t_{stop} - t_{max}) \quad (8)$$

with t_{max} the time at which velocity is maximum and $(t_{stop} - t_{start})$ the total duration of the slider motion during one event. Creep motion is estimated with the theoretical sliding duration T (Sec. I) to avoid that errors made on τ_{slip} estimate impact the corresponding values of τ_c for the same event. Figs. 6c and 6d display the empirical probability density function (PDF) of τ_{sl}/T for the nonlinear and linear filtering. Although slightly shifted toward lower values due to the sharp end of the sliding motion after filtering, data obtained with the nonlinear

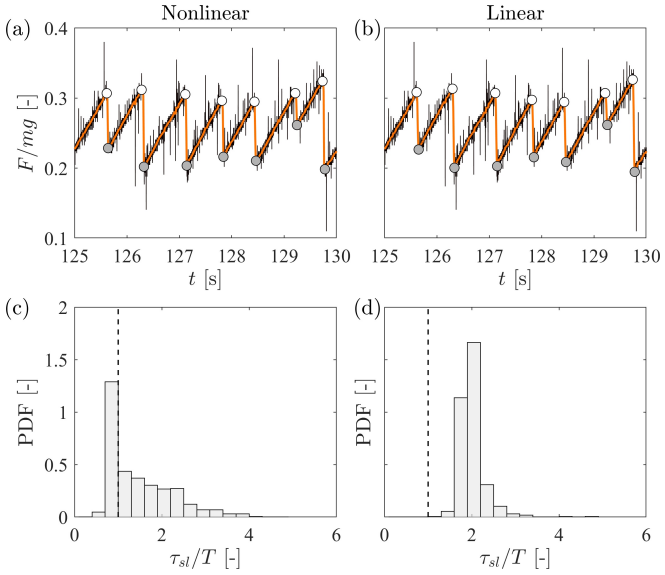


FIG. 6. Nonlinear vs. linear filtering in the stick-slip regime. (a,b) Normalized force signal for the nonlinear (a, $\lambda = 0.8$) and linear (b, $\lambda = 10^4$) filtering. (c,d) Probability density function (PDF) of the slip time τ_{sl} normalized by the theoretical slip time T. The vertical dashed line indicates $\tau_{sl} = T$ [$k = 1002$ N/m, $V = 42$ μm/s].

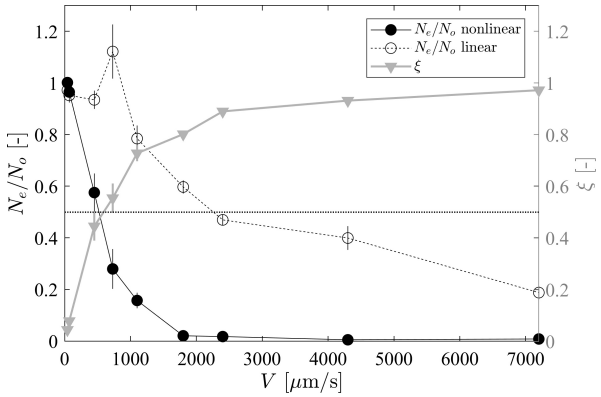


FIG. 7. Number of sliding events normalized by the total number of oscillations N_e/N_o for the nonlinear (solid black line & dots) and the linear (dashed black line & empty dots) filtering as functions of the driving velocity V. The shape of the asymmetry parameter, ξ (gray line & triangles) evidences the relevance of nonlinear filtering (see text). A potentially relevant criterion to quantify the transition between stick-slip and inertial regime is given by $N_e/N_o = 1/2$ [$k = 1002$ N/m].

denoising exhibit a peak close to $\tau_{sl}/T \simeq 1$, as expected in the stick-slip regime. Conversely, the linear filtering overestimates τ_{sl}/T by a factor of about 2, because of the smoothing effect of the short time-scale force drop, not accurately captured by this technique.

3. *Number of events*

The dynamics of the slider can be further characterized by comparing the number of sliding events, N_e against the number of oscillations in the force signal, N_o (defined here as a rise followed by a drop). In the stick-slip regime, at low driving velocity V, N_e equals N_o ($N_e/N_o = 1$), as the slider experiences a rest phase in-between two force drops. When the driving velocity is increased, the slider may experience two or more force rises and drops without coming to rest. In these situations, $N_o > N_e$. Consequently, upon increase of the velocity V, N_e/N_0 decreases until reaching 0 for inertial motion.

Fig. 7 displays N_e/N_o, measured after nonlinear and linear filtering, as a function of the driving velocity V. For the same number of oscillations in the force signal, the linear filtering yields a much larger number of detections of sliding events. Indeed, the smoothing of the force signal induced by the linear filtering not only artificially decreases the sliding velocity (Sec. III B 2) but also tends to decrease the rising slopes of the force signal. As a consequence, the estimated velocity decreases and, in some cases, can go below the threshold for motion detection: a stop phase is attributed to the slider, while it only experiences deceleration and slow motion.

To quantify the ability of the nonlinear filtering to capture the dynamics of the slider, we introduce a parameter ξ characterizing the asymmetry of the velocity signal, computed as the ratio of the time during which the slider velocity is above its average (i.e. the driving velocity V) to the time during which the slider velocity is smaller than V:

$$\xi = \frac{\int H(\dot{x} - V)\mathrm{d}t}{\int H(V - \dot{x})\mathrm{d}t} \tag{9}$$

where H denotes the Heaviside function and the integral is performed over the total signal duration. For small V, the slider exhibits a stick-slip motion and is at rest most of the time, hence $\xi \simeq 0$. Increasing V induces an increase in ξ. At large V, the slider is continuously in motion, and spends half the time above and half the time below V, which leads to $\xi = 1$. Fig. 7 displays ξ as a function of V (gray curve and triangles). When computed after the nonlinear filtering, ξ shows an excellent agreement in shape with the expected anti-correlation with the ratio N_e/N_o. This is far less the case with the linear filtering. In addition, both ξ and N_e/N_o show no strong discontinuities as functions of V, indicating the absence of a sharp transition between the stick-slip and inertial regimes in the paper-paper friction. To characterize the evolution from stick-slip to inertial motion, a potentially relevant criterion is $N_e/N_0 < 1/2$ or $\xi > 1/2$. Both criteria are observed to reach the 50% threshold at about the same critical velocity V_c, a very satisfactory outcome of using the nonlinear filtering to characterize the slider dynamics.

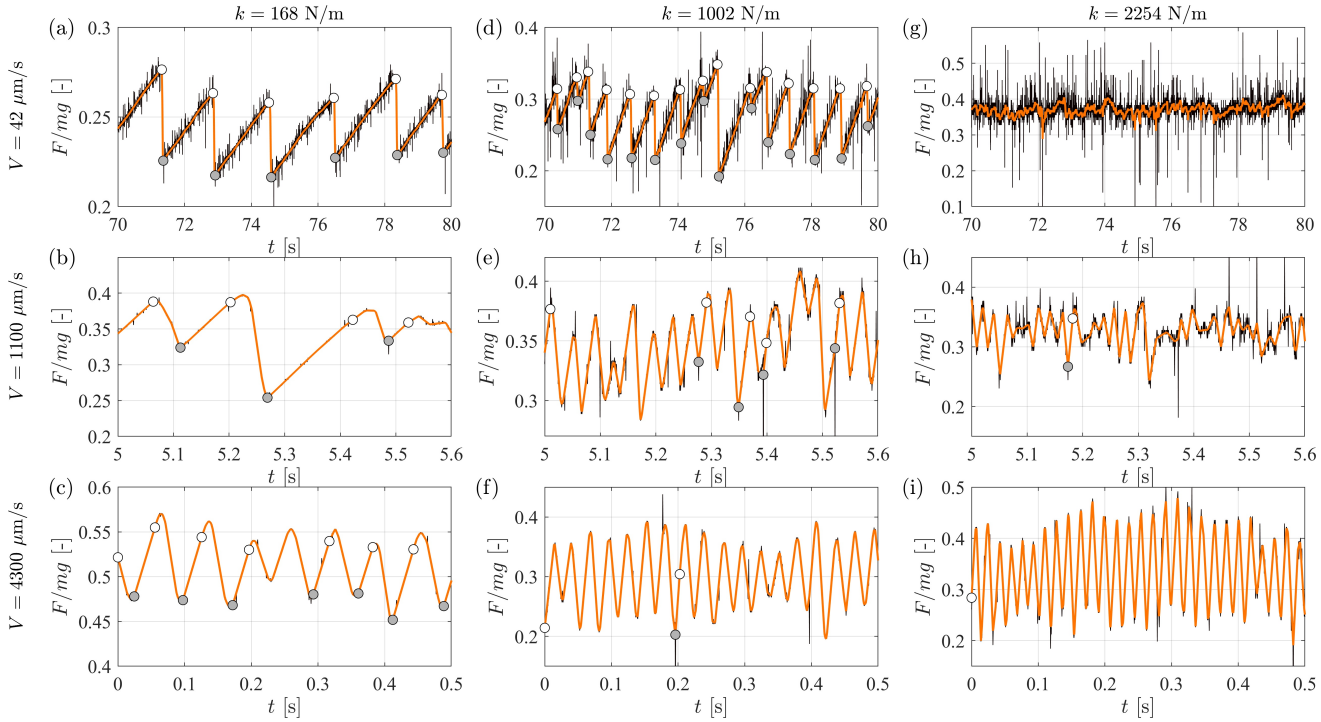


FIG. 8. Dimensionless force F/mg as a function of time, for different spring stiffness (a-c) $k = 168$ N/m, (d-f) $k = 1002$ N/m, (g-i) $k = 2254$ N/m and three different driving velocities (a,d,g) $V = 42$ μm/s, (b,e,h) $V = 1100$ μm/s, (c,f,i) $V = 4300$ μm/s. The white and gray dots indicate the beginning and end of sliding events, detected automatically after nonlinear filtering. The signal at large k and small V (g) is characteristic of continuous sliding (see text). All panels in this figure can be reproduced using the toolbox provided in Supplemental Material.

IV. FRICTIONAL REGIMES CHARACTERISTICS & PHASE DIAGRAM

The previous section clearly established both qualitatively and quantitatively the benefits of the nonlinear filtering compared to the linear filtering in capturing features of the force signal relevant for the analysis of friction dynamics. The nonlinear filtering is thus now systematically applied to the analysis of all 189 recordings, with the aim to characterize the different frictional regimes encountered in the proposed solid friction experiment.

A. Different regimes

Fig. 8 displays the dimensionless force F/mg as a function of time for different values of the spring stiffness k and driving velocity V. For $k = 1002$ N/m (middle column), at small velocity, the system exhibits a clear stick-slip regime (Fig. 8d). When the driving velocity is increased, the slider has less and less stick phases (several oscillations without any stop, Fig. 8e,f). The force signal oscillations become more and more symmetric, a characteristic of the inertial regime. For smaller k (left column, Fig. 8), the driving velocity has to be larger to trigger the inertial regime, while for large k (right column, Fig. 8), a clear inertial behavior without any stick phase is reported (Fig. 8i).

For large k and small V, the signal-to-noise ratio is very small (Fig. 8g). This type of signals is characteristic of continuous sliding in which no more oscillations are reported, often associated with a steady creep of the slider [11, 14, 26]. The nonlinear filtering successfully removes impulsive noise from the normalized force signal (Fig. 8g). This regime can be easily recognized either by eye or by a spectral analysis (not performed here). The slider is always in motion, and no further analysis is performed.

B. Creep motion statistics

Creep motion in the stick-slip regime (typically for $V \leq 70$ μm/s) is analyzed. Fig. 9 displays the empirical probability density function of the creep duration, τ_c, for different values of the control parameters (k, V). The dashed line indicates, as a reference, the theoretical sliding time, T, independent of V, which decreases as k is increased (Sec. I). Interestingly, the average duration of the creep motion, $\tau_c \sim 0.01 - 0.02$ s, does not exhibit any significant dependence on the parameters (k, V). Due to the slow motion of the slider in the creep regime, this characteristic time probably depends on the properties of the material and on the tangential stress only.

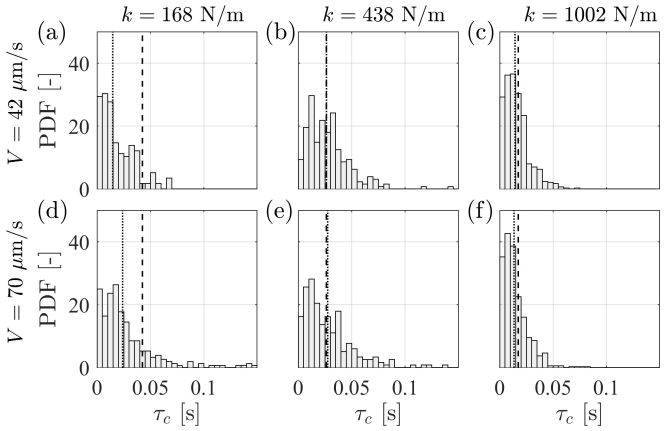


FIG. 9. Histograms of τ_c for different driving velocities and stiffness. The vertical dashed lines point the theoretical sliding time, T, as a reference. The vertical dotted lines correspond to the average value of τ_c for each distribution.

C. Transition to the inertial regime

Further, creep and slip motions are combined, and phases during which the slider is at rest (duration τ_{st}) or in motion (duration τ_m, including possible creep) are characterized, thus making possible the definition of a criterion that quantifies the transition between the stick-slip and inertial regimes. The signals shown in Fig. 8 suggest a dispersion of the frictional properties of the material, for which a visual proxy may consist of the variations in the maximum and minimum values of the normalized force F/mg. Such variations are hence directly reflected in the variations of the times associated with the stick and motion phases, τ_{st} and τ_m (Fig. 1). To account for this variability and to further investigate the transition between the stick-slip and inertial regimes, Fig. 10 displays the distributions of τ_{st}/T and τ_m/T for several driving velocity V. At small velocity (Fig. 10a,b), τ_m/T exhibits a clear peak around 1. The peak is, however, not exactly located at 1, as the motion includes creep, thus shifting τ_m/T towards larger values (inset, Fig. 10a). The distribution of τ_{st}/T displays larger variations: It is broadly extended to small velocities. When V is increased, the distributions get narrower and their average tends to 1, i.e. the duration of the stick phase becomes of the order of the duration of the slip phase, without any creep. Above a threshold velocity (between 70 and 450 μm/s), the slider can remain in motion during several characteristic times T, and experiences successive accelerations and decelerations before coming again to rest. We observe that the distribution of τ_m broadens whereas the average of the stick time τ_{st} gets smaller and smaller. These changes in the distributions point out that the slider is no longer in the regular stick-slip regime.

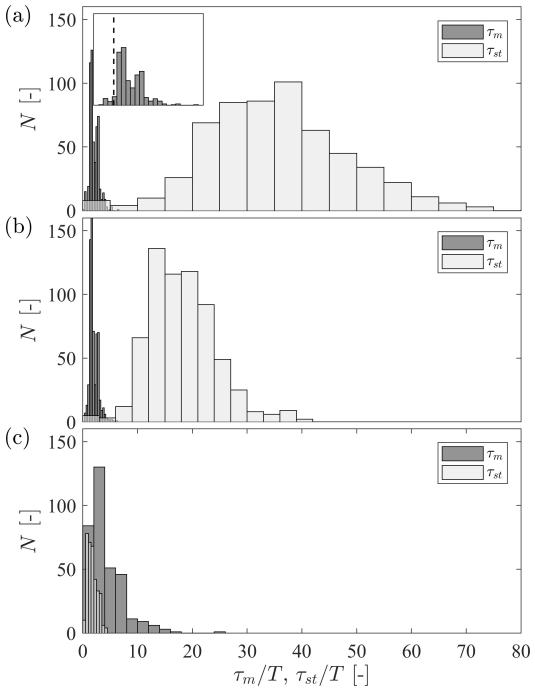


FIG. 10. Histograms of τ_{st}/T (light gray) and τ_m/T (dark gray) (with T the theoretical sliding time in stick-slip regime, see text) for different driving velocities (a) $V = 42$ μm/s, (b) $V = 70$ μm/s, (c) $V = 450$ μm/s. The inset in (a) is a zoom on the peak of τ_m/T distribution. The dashed line indicates $\tau_m/T = 1$ [$k = 1002$ N/m].

D. Phase diagram

To quantify the different regimes, based on the determination of τ_{st} and τ_m, we compute $\mathcal{P}_m$, the fraction of time during which the slider is in motion over the experimental run. For some sets of control parameters (k, V), as discussed previously, the slider experiences a continuous sliding and the denoising technique presented here fails in recovering the signal characteristics, although it captures well its variations (Fig. 8g). Indeed, in these cases, impulsive noise dominates, leading to wrong determination of τ_m and τ_{st}. For these regimes, which are easily identified by eye, $\mathcal{P}_m$ is set to 100%.

We report in Fig. 11 a phase diagram that summarizes the different dynamics revealed by the analysis of the present paper-paper friction experiment under small normal load. In this diagram, CS denotes the continuous sliding regime; SS the stick-slip regime in which the slider is in the stick phase at least 50% of the time; IR the inertial regime in which the slider experiences motion at least 50% of the time; and IR$^+$ the pure inertial regime in which the slider is never at rest and exhibits a steady oscillatory motion. Although this phase diagram attempts to assess boundaries between regimes, transitions found from experimental data are smooth. Except for the continuous sliding regime, the symbols displayed in Fig. 11 may depend on the definition of the stick-slip

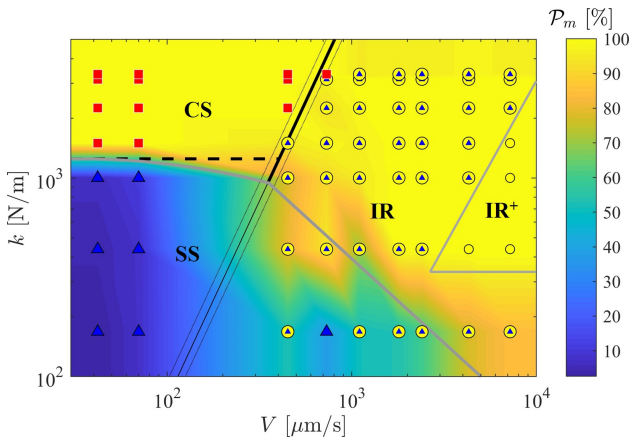


FIG. 11. Phase diagram (k, V) summarizing the different regimes for the dynamics of paper-paper friction [CS = continuous sliding; SS = stick-slip; IR = inertial regime; IR$^+$ = 100% inertial]. The background color represents $\mathcal{P}_m$, the percentage of time the slider spends in motion [Red squares indicate continuous sliding, blue triangles $\mathcal{P}_m < 50\%$, yellow disks including blue triangle $\mathcal{P}_m > 50\%$ and yellow disks $\mathcal{P}_m = 100\%$, the black lines are from the heuristic model and gray lines only guides to the eye].

and inertial regimes (SS and IR are defined based on an arbitrary 50% time criterion). Only the region denoted IR$^+$ exhibits a pure inertial regime as shown in Fig. 1c, without any rest phase of the slider ($\mathcal{P}_m = 100\%$).

It is of particular interest to compare this diagram to the previous results by Heslot *et al.*, obtained with a similar system, but at much larger normal load [11]. Note first that the phase diagram is qualitatively the same, with a stick-slip regime at both small stiffness k and velocity V. Their analysis of the system is based on the fact that the friction coefficient depends logarithmically on the slider velocity $\dot{x}$ [27]. They suggest to write, at small slider velocity $\dot{x}$, as long as the dynamics is primarily governed by slow contact relaxation and creep phenomena, the friction coefficient in the form

$$\mu_d = a + b \ln\left(\frac{D_0}{\dot{x}}\right) \tag{10}$$

where D_0 is a microscopic length that characterizes the surfaces in frictional contact. This small velocity approximation of μ_d holds true as long as the typical contact time $D_0/\dot{x}$ is large compared to the inertial time $\sqrt{m/k}$. The associated boundary corresponds to the transition from CS to IR in which the slider is continuously in motion with $\dot{x} \sim V$. From the thick black line in Fig. 11, we get $D_0 = (2.0 \pm 0.2)$ μm (extreme values are indicated by the dotted lines on both sides). Note that the same transition line could be used to distinguish two regimes in the SS region as done in [11]. We observe that, on the left of the boundary (small V), that the system spends a majority of the time in the stick-slip regime whereas, on the right (large V) it spends a majority of the time in the inertial regime. However the transition is continuous and poorly marked (thin black line). It is rather characterized by the probability map. Let us comment that the lengthscale D_0 is of the order of the micrometer, as found by Heslot *et al.* for another type of paper. Moreover, D_0 is of the order of the typical diameter of the paper fiber, in agreement with its physical origin.

The equation (10) can be used at small V to determine the critical stiffness k_c at the transition between SS and CS regimes [11]

$$k_c = \frac{m\,g}{D_0}\,b\ . \tag{11}$$

From the experimental diagram, we infer $k_c = (1250 \pm 250)$ N/m (horizontal dashed black line) from which we get $b \simeq 8.3\,10^{-3}$. This value, which is of the same order of the value in [11], corresponds to a reasonable decrease of the friction coefficient by 0.06 ($\sim 20\%$) from rest to 1 mm/s. Note that experimentally k_c is not constant and decreases when V is increased (thick gray curve): this trend is due to higher order terms in the dependence of μ_d on $\dot{x}$ and could be, in principle, determined theoretically provided the knowledge of $\mu_d(\dot{x})$.

Finally, the phase diagram must be complemented by the boundary between the SS and the IR regime (thick grey line) for which we do not have any theoretical background. The behavior of the system around this transition is rather complex, the system exhibiting hysteresis and being sensitive to noise [11]. In addition, we can also add to this diagram a guide to the eye around the region, IR+, of pure inertial regime.

V. CONCLUSION

A nonlinear filtering technique relying on recent nonsmooth optimization formulation was shown to permit to relevantly characterize force signals and solid (paper-paper) friction dynamics. It makes it possible, in the stick-slip regime, to capture the slider velocity asymmetry and, thus, the creep motion before sliding. Creep is therefore correctly accounted for as motion. This makes it possible to estimate accuratly the time spent by the slider in the stick regime (τ_{st}) or in motion (τ_m). Large size statistics on the signals show that (i) the creep motion duration is constant in average, independently of (k, V); (ii) although peaked, the distributions of τ_{st} and τ_m are broad, indicating important variations of the frictional properties of the paper in space (heterogeneities) and time (possible sample wear due to shear). Using the fraction of time spent in motion, $\mathcal{P}_m$, a tentative phase diagram for the dynamics of solid paper-paper friction was proposed. Based on the qualitative similarities with the phase diagram for paper-paper friction under larger normal load [11], we can conclude that even at low confinement pressure, the macroscopic friction is driven by microscopic contacts. In addition, this complete phase diagram makes it possible, for the first time, to quantify

the continuous transition between the stick-slip and inertial regime. Further work will be required to assess the universality of such diagram.

The Matlab® toolbox developed in the framework of this study for nonlinear and linear filtering is available as Supplementary Material, and can be downloaded and used by readers interested in denoising raw experimental data on friction (or other) experiments.

ACKNOWLEDGMENTS

This work was supported by Defi Imag'in CNRS SIROCCO, Programa de Cooperación Científica ECOS/CONICYT C14E07 and the Laboratoire International Associé "Matière : Structure et Dynamique" (LIA-MSD, France-Chile).

[1] I.A. Hutchings, Wear **360–361**, 51 (2016)
[2] Y. Desplanques, SAE Int. J. Mater. Manf. **8**(1), 98 (2015)
[3] L. Bureau, T. Baumberger, C. Caroli, O. Ronsin, C. R. Acad. Sci. Paris **2**(IV), 699 (2001)
[4] T. Baumberger, C. Caroli, Adv. Phys. **55**(3-4), 279 (2006)
[5] J.R. Rice, S.T. Tse, J. Geophys. Res. **91**(B1), 521 (1986)
[6] C. Marone, Ann. Rev. Earth Planet. Sci. **26**, 643 (1998)
[7] J.R. Rice, N. Lapusta, K. Ranjith, J. Mech. Phys. Solids **49**, 1865 (2001)
[8] J.H. Dieterich, B.D. Kilgore, Pure Appl. Geophys. **143**, 283 (1994)
[9] L. Rivera, H. Kanamori, Geophys. Res. Lett. **29**(6), 1088 (2002)
[10] E. Wandersman, R. Candelier, G. Debrégeas, A. Prevost, Phys. Rev. Lett. **107**, 164301 (2011)
[11] F. Heslot, T. Baumberger, B. Perrin, B. Caroli, C. Caroli, Phys. Rev. E **49**(6), 4973 (1994)
[12] F. Lacombe, S. Zapperi, H.J. Herrmann, Eur. Phys. J. E **2**, 181 (2000)
[13] S. Nasuno, A. Kudrolli, A. Bak, J.P. Gollub, Phys. Rev. E **58**(2), 2161 (1998)
[14] T. Baumberger, F. Heslot, B. Perrin, Nature **367**, 544 (1994)
[15] S. Mallat, *A wavelet tour of signal processing: The sparse way* (Academic Press, 2008). 832 p.
[16] P.L. Combettes, J.-C., Pesquet, in *Fixed-Point Algorithms for Inverse Problems in Science and Engineering*, ed. by H.H. Bauschke, R.S.B.P.L. Combettes, V. Elser, D.R. Luke, H. Wolkowicz (Springer-Verlag, New York, 2011), pp. 185–212
[17] A. Papoulis, in *Signal analysis*, author=Papoulis, Athanasios, vol. 191, McGraw-Hill New York (1977)
[18] N. Pustelnik, A. Benazza-Benhayia, Y. Zheng, J.C. Pesquet, Wiley Encyclopedia of Electrical and Electronics Engineering (2016)
[19] A. Chambolle, T. Pock, J. Math. Imaging Vis. **40**, 120 (2011)
[20] H.H. Bauschke, P.L. Combettes, *Convex Analysis and Monotone Operator Theory in Hilbert Spaces* (Springer, New York, 2011)
[21] D.L. Donoho, IEEE T. Inform. Theory **41**(3), 613 (1995)
[22] J. Frecon, N. Pustelnik, N. Dobigeon, H. Wendt, P. Abry, IEEE T. Signal Proces. **65**(19), 5215 (2017)
[23] A. Benazza-Benyahia, J.C. Pesquet, IEEE T. Image Process. **14**(11), 1814 (2005)
[24] S. Ramani, T. Blu, M. Unser, IEEE T. Image Process. **17**(9), 1540 (2008)
[25] C.A. Deledalle, S. Vaiter, J. Fadili, G. Peyré, SIAM J. Imaging Sci. **7**(74), 2448 (2014)
[26] T. Baumberger, C. Caroli, B. Perrin, O. Ronsin, Phys. Rev. E **51**(5), 4005 (1995)
[27] C.H. Scholz, *The Mechanics of Earthquakes and Faulting* (Cambridge University, 1990), Chap. 2 and references therein